Multistable Metamaterial on Elastic Foundation Enables Tunable Morphology for Elastic Wave Control

V. Ramakrishnan[1] and M. J. Frazier[1, a)]
Department of Mechanical and Aerospace Engineering, University of California, San Diego, California 92093, USA

(Dated: 23 September 2020)

We present a strategy for continuously and reversibly tuning the propagation of elastic waves in one-dimensional systems without need for persistent external stimulation. The general approach places a bistable metamaterial on an elastic substrate which is subsequently deformed via prescribed boundary displacements. The internal substrate deformation, which is shaped by a prescribed spatial variation in elasticity, is reflected in the overlaying metamaterial and facilitates the reconfiguration of bistable elements over isolated regions. As each configuration is associated with a unique stiffness, these regions represent an adjustable, meso-scale morphology amenable to tuning elastic waves. The essential bistability is characterized by an asymmetric, double-welled equipotential energy function and is developed by mechanical rather than phenomenological means. The asymmetry provides for the unique, configuration-specific (stable) equilibrium stiffnesses; the equipotential promotes reversibility (i.e., no one configuration is energetically preferred). From a uniform metamaterial-substrate system, we demonstrate the utility of our strategy by producing a waveguide with shifting pass band and a metamaterial with variable unit cell morphology.

I. INTRODUCTION

Architected metamaterials[1–3] are remarkable for their extraordinary thermal[4–6], mechanical[7–9], acoustic[10–15], and optical[16,17] performance stemming from a cleverly designed internal architecture, comprising both a characteristic (often periodic) structural geometry and constituent material morphology – in a sense, representing the emancipation of material behavior from the limitations of chemistry. In particular, research pertaining to elastic wave propagation has realized extreme/counterintuitive effective properties[8,18] that bring once fantastic applications into practical reach[19–22]. In addition, illustrating a broad range of applicable scales, new strategies for, e.g., thermal management[23,24], signal processing[25], acoustic sensing[26], energy harvesting[27–29], and earthquake mitigation[30,31] have also been proposed.

However, utilizing "stiff" material constituents in the metamaterial construction leaves little opportunity to adapt the dynamic performance for scenarios where the target frequency range may fluctuate significantly (e.g., as in environmental vibration mitigation and energy harvesting applications), thus limiting effectiveness outside a fixed service range. One remedy is the class of active architectures which leverage shunted piezoelectric elements[32–37] to adjust the effective stiffness via electromechanical coupling, thus tuning the native dispersion characteristics of the metamaterial. Nevertheless, it is conceivable that for certain metamaterial applications, obviating the need for the accompanying complex wiring and external controllers is desirable. Serving to accommodate this requirement, a second approach toward inherently tunable performance utilizes soft material constituents for which deforming the internal architecture modifies the effective stiffness and, consequently, the characteristic wave dispersion. By exploiting instability and multistability in readily re-configurable soft architectures, efforts to imbue metamaterials with an inherent tuning capability, generally, effect one of two outcomes: (i) the tuning is continuous and reversible, though the tuned configurations are reliant on the constant support of an external field or prescribed boundary condition[38–45] or (ii) the tuning is among a finite number of discrete, stable configurations, though the process is energetically fated to follow an energy-minimizing sequence[46–52], prohibiting restoration to an earlier configuration; thus, tuning is irreversible and, ultimately, terminated. Continuous tuning allows for small adjustments; reversible tuning facilitates repeated adjustments; and stable tuning eliminates the need for an ever-present supporting field or boundary condition. Xia *et al.*[53] demonstrated these tuning abilities in a silicon-coated microlattice utilizing an electrochemical reaction. A metamaterial system possessing a inherent tuning capability independent of chemistry and external controllers which permits continuous, reversible, and stable adjustments to the dispersion characteristics [i.e., combining the desirable attributes of outcomes (i) and (ii)] is appealing and the aim of the present work.

In this article, we propose a class of architected metamaterial whose effective stiffness as well as its distribution is continuously, stably, and reversibly adjustable for adaptive dynamic performance using the technique of strain engineering. The general strategy couples a soft, multistable metamaterial to a relatively stiff (though deformable) foundation which, when strained, assists in reconfiguring the multistable architecture, modifying the metamaterial performance. A similar approach has been explored in the context of controllable electronic and photonic performance in thin-film materials[54,55]. Following this strategy, the strain state in the elastic substrate is reflected in the overlaying metamaterial, causing isolated regions to switch to the opposing configuration characterized by a unique effective stiffness, i.e., one that is acoustically distinct to the propagating wave. Moreover, dependent upon the strain

a)Electronic mail: mjfrazier@ucsd.edu.

magnitude, the size of the switched regions are customizable, enabling a post-fabrication redistribution of the stiffness property. This redistribution of a mechanical property, achieved without an external controller or appeal to chemistry, adds a second dimension to the tuning operation and is unique to the relevant literature. As the non-convex potential energy landscape is not biased toward a particular configuration, the tuned stiffness patterning in the re-configured metamaterial is stable (permitting quasi-static removal of the instigating boundary displacements) and potentially reversible (requiring the same effort to elicit and reverse the tuned state). In one dimension, we introduce and analyze two such metamaterial systems. While the multistability is localized in one system, it is interactive in another which affects reversibility. In addition, continuous tuning, i.e., that permitting small adjustments in configuration, is demonstrated. Our approach will be applied to the establishment of waveguides with shifting transparency and metamaterial unit cells with tunable (stiffness) morphology.

The remainder of the article is organized as follows: Section II presents simple realizations of our strategy in the form of mass-spring systems, including a qualitative and analytical description of the energetic and dispersion characteristics. In Section III, we analyze and discuss the results of numerical simulations illustrating the tunable wave filtering properties. We demonstrate the concept in the form of (1) a waveguide with an adjustable pass band and (2) a metamaterial with a variable unit cell (stiffness) morphology. Finally, in Sec. IV, we draw insights from the numerical results and suggest avenues for further study.

II. MODEL DESCRIPTION

A. The Asymmetric, Equipotential Function

Figure 1a illustrates the basic structural element giving rise to the metamaterial multistability, representing an elaborated conception of the bistable unit found in related works[49,56]. In part, the bistable element comprises two identical, pin-connected axial springs, k_A, arranged symmetrically about and at an angle to the x-axis as illustrated. This construction ensures that, as the pinned end displaces, u_A, the combined reaction from the axial springs is always parallel to the displacement. A notable distinction with earlier works, the remote ends of each spring are not fixed, but may displace, u_B, along the horizontal axis. Given the relative displacement, $\Delta = (u_A - u_B)/d_x$, the corresponding non-convex potential function, $\psi_A(\Delta)$, is symmetric about the unstable equilibrium configuration, $\Delta = 1$. In addition to $\psi_A(\Delta)$, the total bistable energy has contributions from an elastic potential, $\psi_T(\Delta)$, originating from a pair of torsional springs, k_T, at the remote ends of each k_A, and a magnetic potential, $\psi_M(\Delta)$, stemming from the interaction between a horizontally-aligned magnetic dipole moment, $\mathbf{p}_m$, affixed to pinned end and a pair of dipole moments, $\mathbf{p}_s$, collocated with the torsional springs and oriented an angle, θ, with respect to the x-axis (see Fig. 1a). Together, these contributions foster the crucial asymmetric equipotential necessary for stable, reversible tuning. Specifically, the total bistable potential

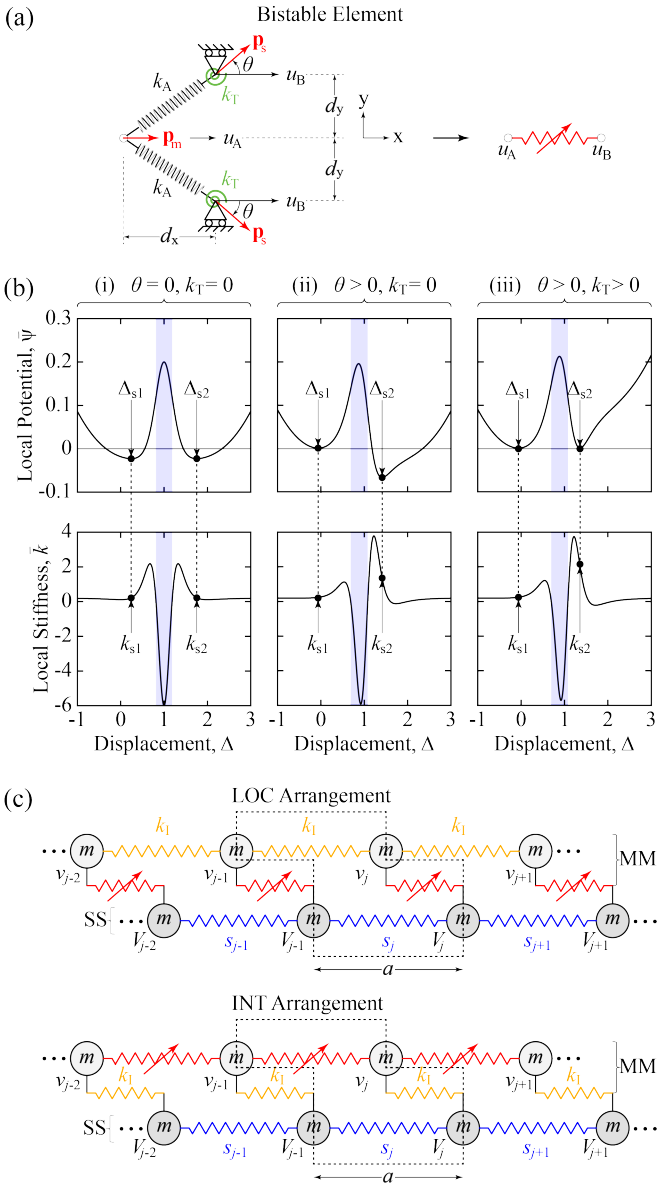

FIG. 1. (Color online). Bistable Metamaterial on Elastic Foundation. (a) The essential bistable element of the metamaterial-substrate systems. (b) The non-convex energy function is adjusted by the geometric and material parameters to yield an asymmetric, equipotential profile. The asymmetry is reflected in the corresponding stiffness function, resulting in a unique stiffness, $k = \{k_{s1}, k_{s2}\}$, for each of the two equilibrium configurations, $\Delta = \{\Delta_{s1}, \Delta_{s2}\}$. The shaded region identifies the negative stiffness region. (c) Two metamaterial-substrate (MM-SS) arrangements with lattice constant, a: one in which the bistable element is local (LOC) to each metamaterial degree-of-freedom; another in which the bistable element couples two metamaterial degrees-of-freedom (INT). For compact display, the bistable element is represented as a nonlinear spring which is indicated by an arrow.

becomes

$$\psi(\Delta) = \psi_{\rm A}(\Delta) + \psi_{\rm M}(\Delta) + \psi_{\rm T}(\Delta), \tag{1}$$

where the full equations for each component is given in the Appendix. The corresponding stiffness function is given as $k(\Delta) = \partial^2\psi/\partial\Delta^2$. The two stable equilibrium configurations, $\Delta = \{\Delta_{\rm s1}, \Delta_{\rm s2}\}$ ($\Delta_{\rm s1} < \Delta_{\rm s2}$), are characterized by stiffnesses $k = \{k_{\rm s1}, k_{\rm s2}\}$.

Figure 1b illustrates the effect of each component in Eq. (1) on the shape of the bistable energy landscape and stiffness function. While $k_{\rm T} = 0$ and the dipole moments $\mathbf{p}_{\rm s}$ are oriented such that $\theta = 0$, the bistable potential is symmetric [Fig. 1b.(i)]; consequently, $k_{\rm s1} = k_{\rm s2}$. Changing either of these conditions alone, generally, biases the energy landscape toward a specific equilibrium configuration [Fig. 1b.(ii)] and hinders reversible tuning; however, a suitable choice of $k_{\rm T}$ and $\mathbf{p}_{\rm s}$ will produce an asymmetric, equipotential landscape with $k_{\rm s1} \neq k_{\rm s2}$ [Fig. 1b.(iii)].

B. The Governing Equations and Homogeneous Dispersion Relations

Two metamaterial-substrate arrangements are considered, distinguished by the placement of the bistable element within the unit cell of an N-cell chain (schematically represented as a nonlinear spring in Fig. 1c). In one arrangement (LOC), the bistable element couples the local metamaterial and substrate degrees-of-freedom, i.e., $\{u_{\rm A}, u_{\rm B}\} \rightarrow \{v_j, V_j\}$; in another (INT), the bistable element links nearest neighbors in the overlaying metamaterial, i.e., $\{u_{\rm A}, u_{\rm B}\} \rightarrow \{v_{j-1}, v_j\}$. In the preceding statement, the right arrow maps the displacements of the bistable element, $u_{\rm A}$ and $u_{\rm B}$ (Fig. 1a), to those of the metamaterial layer, v, and substrate layer, V (Fig. 1c). The substrate features springs of variable stiffness, s_j, joining neighboring degrees-of-freedom. The variability enables an inhomogeneous strain. In addition, each arrangement features springs, $k_{\rm I}$, which are interactive in the LOC arrangement and local in the INT arrangement.

Dimensionless governing equations will enable the investigation of the dynamics without reference to explicit geometric and material parameters. For this reason, displacements, position, and time are scaled by suitable quantities:

$$\bar{v} = v/d_{\rm x}, \quad \bar{V} = V/d_{\rm x}, \quad \bar{x} = x/a, \quad \bar{t} = \omega_0 t,$$

where $\omega_0^2 = k_{\rm I}/m$. In addition, $k_{\rm I}d_{\rm x}^2$ defines a convenient unit of energy. Thus, for a chain of N unit cells, the dimensionless Lagrangian is

$$\mathscr{L}^{\rm LOC} = \sum_{j=1}^{N}\left[\frac{1}{2}(\dot{\bar{v}}_j^2 + \dot{\bar{V}}_j^2) - \bar{\psi}(\bar{V}_j, \bar{v}_j)\right] - \frac{1}{2}\sum_{j=2}^{N}\left[\bar{s}_j(\bar{V}_j - \bar{V}_{j-1})^2 + (\bar{v}_j - \bar{v}_{j-1})^2\right], \tag{2a}$$

$$\mathscr{L}^{\rm INT} = \frac{1}{2}\sum_{j=1}^{N}\left[\dot{\bar{v}}_j^2 + \dot{\bar{V}}_j^2 - (\bar{v}_j - \bar{V}_j)^2\right] - \sum_{j=2}^{N}\left[\frac{\bar{s}_j}{2}(\bar{V}_j - \bar{V}_{j-1})^2 + \bar{\psi}(\bar{v}_j, \bar{v}_{j-1})\right], \tag{2b}$$

where $\bar{s}_j = s_j/k_{\rm I}$ is the normalized local substrate stiffness and $\bar{\psi} = \psi/k_{\rm I}d_{\rm x}^2$. Accordingly, for an arbitrary unit cell, j, the Euler-Lagrange governing equations stemming from Eqs. (2) are

$$\ddot{\bar{v}}_j + (2\bar{v}_j - \bar{v}_{j-1} - \bar{v}_{j+1}) + \frac{\partial\bar{\psi}(\bar{V}_j, \bar{v}_j)}{\partial\bar{v}_j} = 0, \tag{3a}$$

$$\ddot{\bar{V}}_j + \bar{s}_j(\bar{V}_j - \bar{V}_{j-1}) + \bar{s}_{j+1}(\bar{V}_j - \bar{V}_{j+1}) + \frac{\partial\bar{\psi}(\bar{V}_j, \bar{v}_j)}{\partial\bar{V}_j} = 0. \tag{3b}$$

for the LOC arrangement and

$$\ddot{\bar{v}}_j + (\bar{v}_j - \bar{V}_j) + \frac{\partial\bar{\psi}(\bar{v}_j, \bar{v}_{j+1})}{\partial\bar{v}_j} + \frac{\partial\bar{\psi}(\bar{v}_j, \bar{v}_{j-1})}{\partial\bar{v}_j} = 0, \tag{4a}$$

$$\ddot{\bar{V}}_j + (\bar{V}_j - \bar{v}_j) + \bar{s}_j(\bar{V}_j - \bar{V}_{j-1}) + \bar{s}_{j+1}(\bar{V}_j - \bar{V}_{j+1}) = 0, \tag{4b}$$

for the INT arrangement. In the simulations to follow, Eqs. (3) and (4) are used to model the response of the system to prescribed substrate boundary displacement.

To evaluate harmonic wave propagation in the overlaying metamaterial, we assume $\bar{s}_j$ is such that the substrate is comparatively rigid so that any disturbance propagating within the metamaterial does not transfer a meaningful portion of its energy into the substrate. Thus, we need only consider Eqs. (3a) and (4a) in the analysis. For the simplest case of a homogeneous metamaterial (i.e., bistable elements in identical configuration), the application of Bloch's theorem provides the characteristic dispersion relations for the LOC and INT arrangements, respectively, (see Appendix)

$$2 + \bar{k}_{{\rm s}(i)} - \frac{1}{\gamma} - \gamma = \bar{\omega}^2, \quad \text{(LOC)} \tag{5a}$$

$$1 + \bar{k}_{{\rm s}(i)}\left(2 - \frac{1}{\gamma} - \gamma\right) = \bar{\omega}^2, \quad \text{(INT)} \tag{5b}$$

where $\bar{\omega} = \omega/\omega_0$ is the normalized wave frequency and $\gamma = \exp(\mathrm{i}\kappa a)$ the propagation constant with dimensionless complex wavenumber, κa. In solving Eqs. (5) for γ, the real (propagating) and imaginary (attenuating) components of the complex wavenumber are extracted as: $\kappa_{\rm R}a = |\mathrm{Re}\,(\mathrm{i}\ln\gamma)|$ and $\kappa_{\rm I}a = |\mathrm{Im}\,(\mathrm{i}\ln\gamma)|$.

III. NUMERICAL RESULTS

For analysis, the material and geometric parameters contained in Table I are utilized and are unique to each system. As detailed in the Appendix, the parameters define the bistable potential function, $\bar{\psi}$. Consequently, for both the LOC and INT arrangements, $\bar{k}_{s2}/\bar{k}_{s1} = 10$. Figure 2 displays the arrangement-specific dispersion curves for the metamaterial uniformly in each of the two stable configurations. The configuration-specific frequency ranges over which the metamaterial supports propagating waves begins to illustrate the anticipated performance tuning capability.

In the following subsections, respectively, we utilize substrates with constant and periodic spatial variation in stiffness, $\bar{s}_j$, to re-configure the overlaying metamaterial and alter its dynamic performance in the context of wave propagation. These will be applied to the establishment of waveguides with shifting transparency and metamaterials with tunable pass bands.

A. Waveguide with Shifting Transparency

To demonstrate the enhanced functionality acquired by a bistable metamaterial coupled to a strained elastic substrate, we first study the case of a homogeneous foundation, i.e., $\bar{s}_j = \text{const}$. We consider a chain of $N = 50$ unit cells and, without loss of generality, initiate each bistable element in the first stable configuration, Δ_{s1}; thus, the original, untuned metamaterial is characterized by the stiffness, $\bar{k}_{s1}$. Prescribed displacements are applied quasi-statically to the substrate boundaries, establishing a uniform internal strain, $\varepsilon = (\bar{V}_N - \bar{V}_1)/N$. As a consequence of substrate coupling, the metamaterial simultaneously deforms, effecting switching in certain bistable elements. Subsequently, the boundary displacements are quasi-statically removed, leaving a stable pattern of original and re-configured bistable elements which establishes the tuned metamaterial.

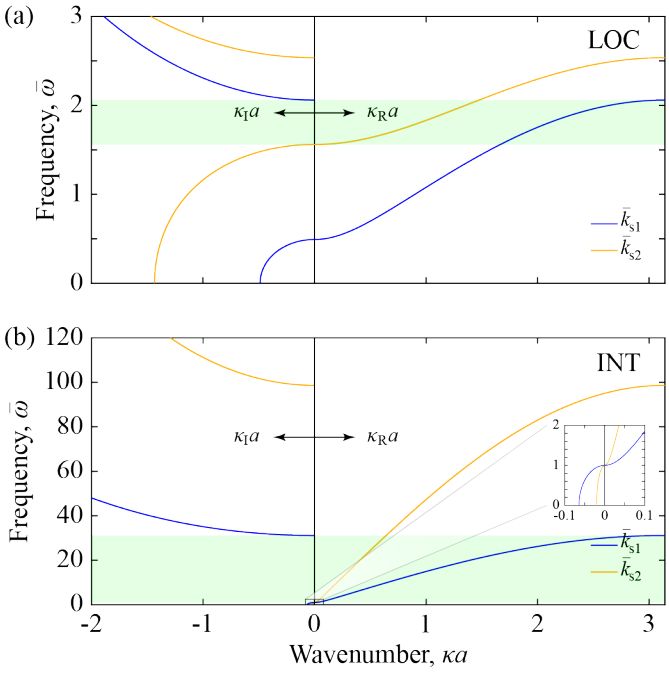

FIG. 2. Dispersion Diagram. For an asymmetric bistable potential, the equilibrium stiffnesses are, generally, distinct, producing unique dispersion diagrams. In the above, the shaded region identifies the shared frequency range of the configuration-specific pass bands. The inset shows the frequency region of the lower band gap.

For the LOC arrangement, the k_I resist the metamaterial deformation, leading to a relative displacement between the local metamaterial and substrate degrees-of-freedom, $\Delta_j = \bar{v}_j - \bar{V}_j$, which changes signs about the midpoint of the mass-spring chain. Thus, switching is facilitated in bistable elements on one half of the metamaterial (especially closer to the boundary) and hindered in those elements on the opposite half. At most, substrate strain may re-configure only half of the bistable elements in the chain. A single domain wall separates the original and the switched elements, each characterized by acoustically distinct stiffnesses, $\bar{k}_{s1}$ and $\bar{k}_{s2}$, respectively. These effects are depicted in Fig. 3a for increasing (compressive) substrate strain.

For the INT arrangement, the bistable elements oppose the metamaterial deformation, $\Delta_j = \bar{v}_j - \bar{v}_{j+1}$, which, due to the free metamaterial boundaries, decreases in magnitude from the chain midpoint but does not change sign. Therefore, all elements are susceptible to re-configuration, although elements nearer the metamaterial interior will switch first. In addition, as switching entails $\Delta_j \neq 0$, in the absence of the substrate, the tuned metamaterial would exhibit a lingering deformation (i.e., a residual strain) – the more elements that switch, the greater the effect. However, the substrate counteracts this effect and, since it is rigid (though elastic) compared to the metamaterial, generally, $\Delta_j \neq \Delta_{s(i)}$, as for the LOC arrangement. For the INT arrangement, two domain walls form as a consequence of interior elements switching before those nearer the boundaries; however, since Δ_j deviates from the equilibrium values, $\Delta_{s(i)}$, the local stiffness, $\bar{k}_j$, also deviates from $\bar{k}_{s(i)}$. These effects are depicted in Fig. 3b for increasing (compressive) substrate strain.

To demonstrate the strain-dependent wave dynamics of the tuned metamaterial, Figs. 3c,d display the FFT of the time signal $\bar{v}_{50}(\bar{t})$ following an impulse, $\dot{\bar{v}}_1(\bar{t})\delta(\bar{t} - \bar{t}_0)$, which instigates a propagating disturbance. An absorbing boundary consisting of an additional 200 cells with $\bar{k}_j = \bar{k}_{50}$ $(51 \leq j < 250)$ and linearly increasing damping is utilized. Dependent upon the specific tuned stiffness profile, $\bar{k}_j$, the frequency range over which the metamaterial is transparent to propagating waves shifts. For the LOC arrangement in Fig. 3c, following a substrate strain of $\varepsilon = -6.75 \times$

TABLE I. Material and Geometric Parameters

	$\bar{k}_A$	$\bar{k}_T$	$\bar{k}_M$	δ	ω_0^2
LOC	1/10	187/8791	71/565	2	100
INT	100	1957/92	14200/113	2	1/10

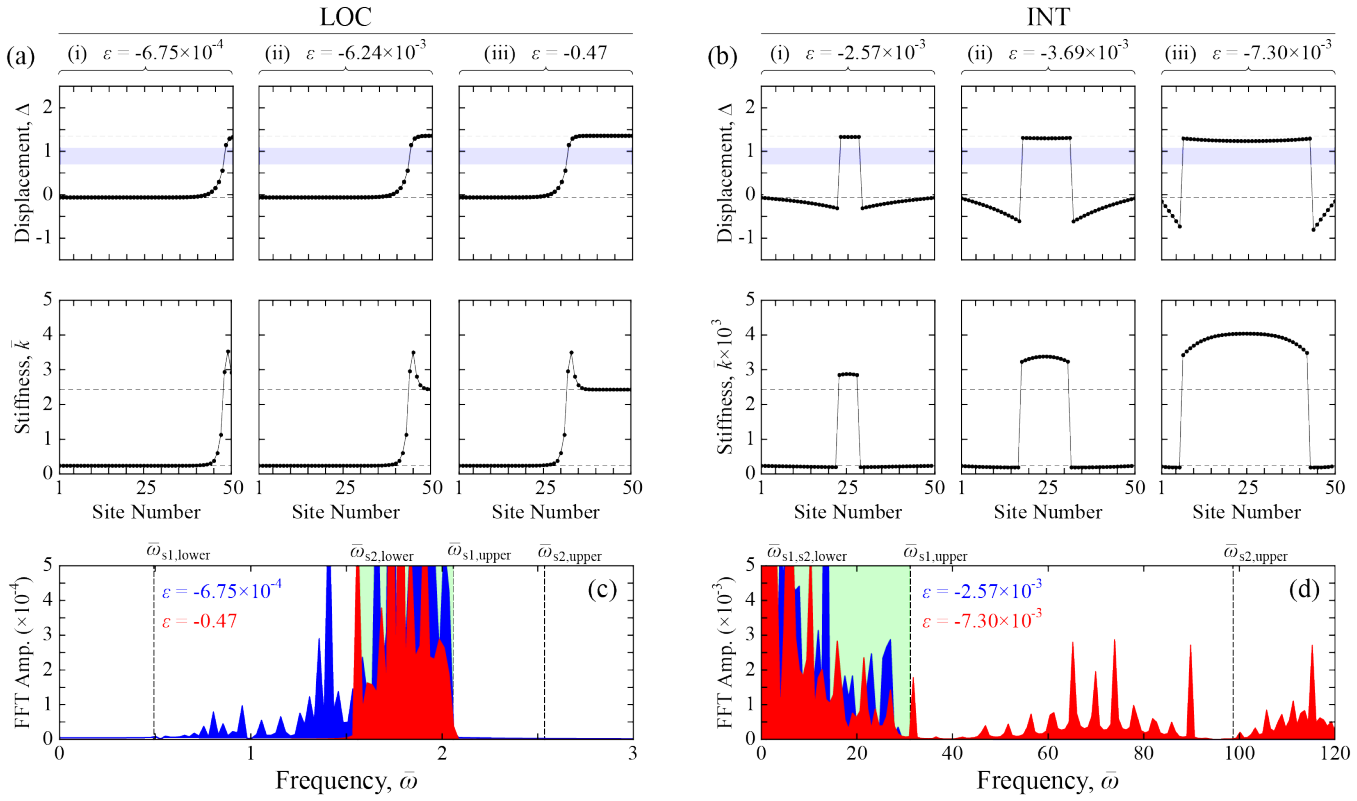

FIG. 3. (Color online). Waveguide with Shifting Transparency. The relative displacement and stiffness profiles of bistable elements in the (a) LOC and (b) INT metamterial-substrate arrangements. The dashed lines identify the stable equilibrium displacements, $\Delta_{s(i)}$, and stiffnesses, $\bar{k}_{s(i)}$. The indicated strain, ε, is that induced in the substrate by a quasi-statically applied (and subsequently removed) boundary displacement. (c,d) The strain-dependent stiffness profile affects the propagation of waves generated by an impulse. This is apparent in the non-coincident Fourier transforms of $\bar{v}_{50}(\bar{t})$ at different strains. The dashed lines represent the upper and lower frequency bounds of the pass bands for the homogeneous Δ_{s1} and Δ_{s2} configurations. The shaded region identifies the shared frequency range of the configuration-specific pass bands

10^{-4}, the metamaterial dynamics is essentially unchanged as few bistable elements are re-configured; consequently, components of the transmitted signal lie within the pass band associated with $\bar{k}_{s1}$ in Fig. 2a. Following a substrate strain of $\varepsilon = -0.47$, the metamaterial exhibits two domains characterized by $\bar{k}_{s1}$ and $\bar{k}_{s2}$, respectively; therefore, the components of the transmitted signal are restricted to the narrower frequency range in which the dispersion curves in Fig. 2a overlap. Outside this range, wave motion is hindered by Bragg scattering and confined to the domain in which the disturbance was generated. A similar effect is observed for the INT arrangement in Fig. 3d where sufficient substrate strain causes most of the bistable elements to switch. Note, however, that the residual strain causes the stiffness profile to deviate from $\bar{k}_{s2}$ in the switched region and so the frequency range of components within the transmitted wave deviates from that indicated by Fig. 2b.

The results depicted in Fig. 3 demonstrate the utility of an elastic substrate for tuning metamaterials with multistable elements: with access to only the substrate boundaries, the multistable elements at the boundary and within the interior may be switched. In contrast, earlier works utilizing multistable elements for tunable metamaterial performance offer no means of switching individual or isolated groups of elements in the interior. For both the LOC and INT arrangements, a strained substrate enables altering the metamaterial morphology (i.e., the stiffness distribution)[57] and, as a result, the transmission of incoming waves.

The manner in which the two arrangements facilitate switching bistable elements impacts the reversibility of the tuned metamaterial configurations. Recall that, for the LOC arrangement, Δ_j exhibits a sign change about the system midpoint, promoting switching in one half of the mass-spring chain and reinforcing the native state it in the other half. From the tuned metamaterial configuration, reversing the substrate strain inverts Δ_j and, thus, the bistable elements in re-configured half are directed back to the native state while those in the native state are switched. Therefore, generally, the LOC arrangement does not support reversible tuning. Alternatively, for the INT arrangement, Δ_j does not exhibit a sign change but is maximum (in magnitude) near the system midpoint, causing switching to commence there. From the tuned metamaterial configuration, inverting Δ_j by reversing the substrate strain returns the switched elements to their native configurations without re-configuring any elements presently in the native configuration. Therefore, generally,

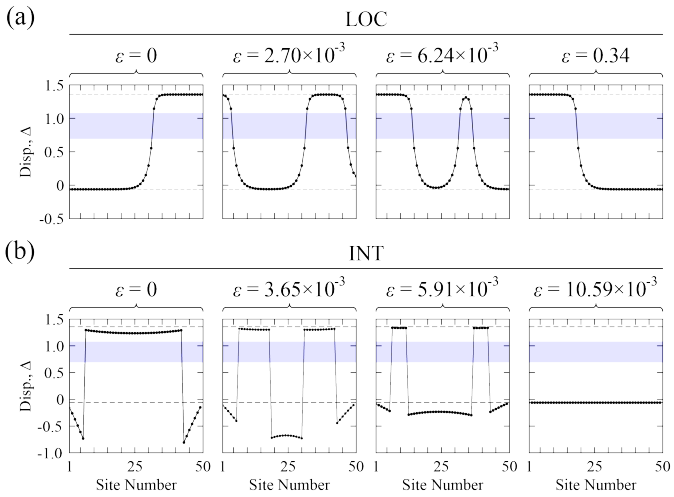

FIG. 4. Reversibility of LOC and INT Arrangements. In response to substrate strain, the relative displacement, Δ_j, exhibits a sign change in the LOC arrangement but not in the INT arrangement. Above, metamaterials in the (a) LOC and (b) INT arrangements are initialized in the tuned configurations in Figs. 3a.(iii) and b.(iii), respectively, which were attained via substrate compression. Subsequently, submitting the substrate to tension reveals the reversibility of tuning the overlaying metamaterial. The INT metamaterial is able to return to its original, untuned state while the LOC metamaterial is not.

the INT arrangement supports reversibility. These effects are observed in Fig. 4 and the Supplemental animations.

B. Unit Cell with Variable Morphology

In the preceding subsection, a homogeneous substrate (i.e., $\bar{s}_j = \text{const.}$) supports a uniform strain distribution which re-configures the bistable elements in the overlaying metamaterial: for the LOC arrangement, switching commences at one of the metamaterial boundaries; for the INT arrangement, switching initiates within the interior. Naturally, substrates with a variable stiffness profile (i.e., $\bar{s}_j \neq \text{const.}$) will alter these results and may deliver an enhanced tuning capability. A substrate with monotonic stiffness function, for example, (not presented here) would permit switching elements in the LOC chain beyond (or short of) the current limit at the chain midpoint and, in the INT chain, would allow switching to initiate at or nearer a boundary rather than the interior. Nevertheless, in the following, we consider an elastic foundation with periodic stiffness function in order the effect a metamaterial with variable unit cell morphology for wave control.

For simplicity, we consider a bi-material substrate with stiffnesses α and β ($\alpha < \beta$) which, as before, are sufficiently large to ensure that the substrate is rigid compared to the overlaying metamaterial. These stiffnesses are distributed periodically within the substrate with a unit cell comprising thirty springs; therefore, the overlaying metamaterial, once tuned, is expected to exhibit the same periodicity. In particular, for the LOC arrangement, $\bar{s}_j = \alpha$ for $j \leq 15$ and $\bar{s}_j = \beta$ for $15 < j \leq 30$; for the INT arrangement, $\bar{s}_1 = \alpha$ and $\bar{s}_j = \beta$ for $1 < j \leq 30$. The interface between the two stiffness regions provides a nucleation site at which switching may commence. Utilizing alternative bi-material distributions or multi-material substrates, isolated regions of the metamaterial may be designed to switch in a pre-determined sequence; nevertheless, this is not present interest. In the following, we consider wave propagation within finite systems consisting of twenty of the earlier defined unit cells.

Figures 5a,b illustrate the state of the bistable elements in the metamaterial for the LOC and INT arrangements, respectively. In particular, the first row shows the relative displacement, Δ_j, for the twenty-cell systems corresponding to the indicated nominal strain induced by boundary displacement. Apparently, the periodic substrate supports an internal strain field with the same periodicity which assists in switching the bistable elements at the same spatial intervals. To the purpose of tunable wave propagation, the second row of each sub-figure, focuses on the variation of the morphology, $\bar{k}_j$, over the unit cell at several levels of substrate strain. Substrate strain changes the distribution of the bistable stiffness within the unit cell which impacts the metamaterial dispersion characteristics.

We compute the dispersion curves utilizing the stable, strain-dependent metamaterial unit cells. In each stable configuration, following the definition in Sec. II. A., the local stiffness $\bar{k}_j = k(\Delta)$ is determined at each jth element of the re-configured unit cell, and then a dispersion analysis is performed for the system of $N = 30$ elements by suitably extending Eqs. (3) and (4) and apply Bloch's theorem, $\bar{v}_1 = \bar{v}_{30}\gamma$ (see Appendix). Figures 5c,d show how the frequency range of pass bands, respectively, in the overlaying LOC and INT metamaterials change as a function of substrate strain. We also determine the FFT of the time signal $\bar{v}_{600}(\bar{t})$ following an impulse, $\dot{\bar{v}}_1(\bar{t})\delta(\bar{t} - \bar{t}_0)$. Again, an absorbing boundary with $\bar{k}_j = \bar{k}_{600}$ ($601 \leq j < 800$) and linearly increasing damping is utilized. For a particular strain, we compare the computed dispersion and the FFT from time simulation. For both the LOC and the INT arrangement, there is excellent agreement between the analytical and numerical results. These results, together with those of the previous section, support the notion of inherent and tunable wave control via an adjustable material morphology. Comparing the common frequency regions in the FFTs in Figs. 3c,d and 5c,d, we notice that periodic distributions of $\bar{k}_j$ opens additional band gaps, illustrating the impact of the present repeating morphology with respect to the relatively simple variations in Sec. III A. Although, the overlaying metamaterial in the LOC arrangement is capable of stable and continuous tuning, except for a narrow range of tuned configurations, it is irreversible. However, in the case of an INT-type system, the tuning processes is able to meet all three requirements – stable, reversible, and continuous.

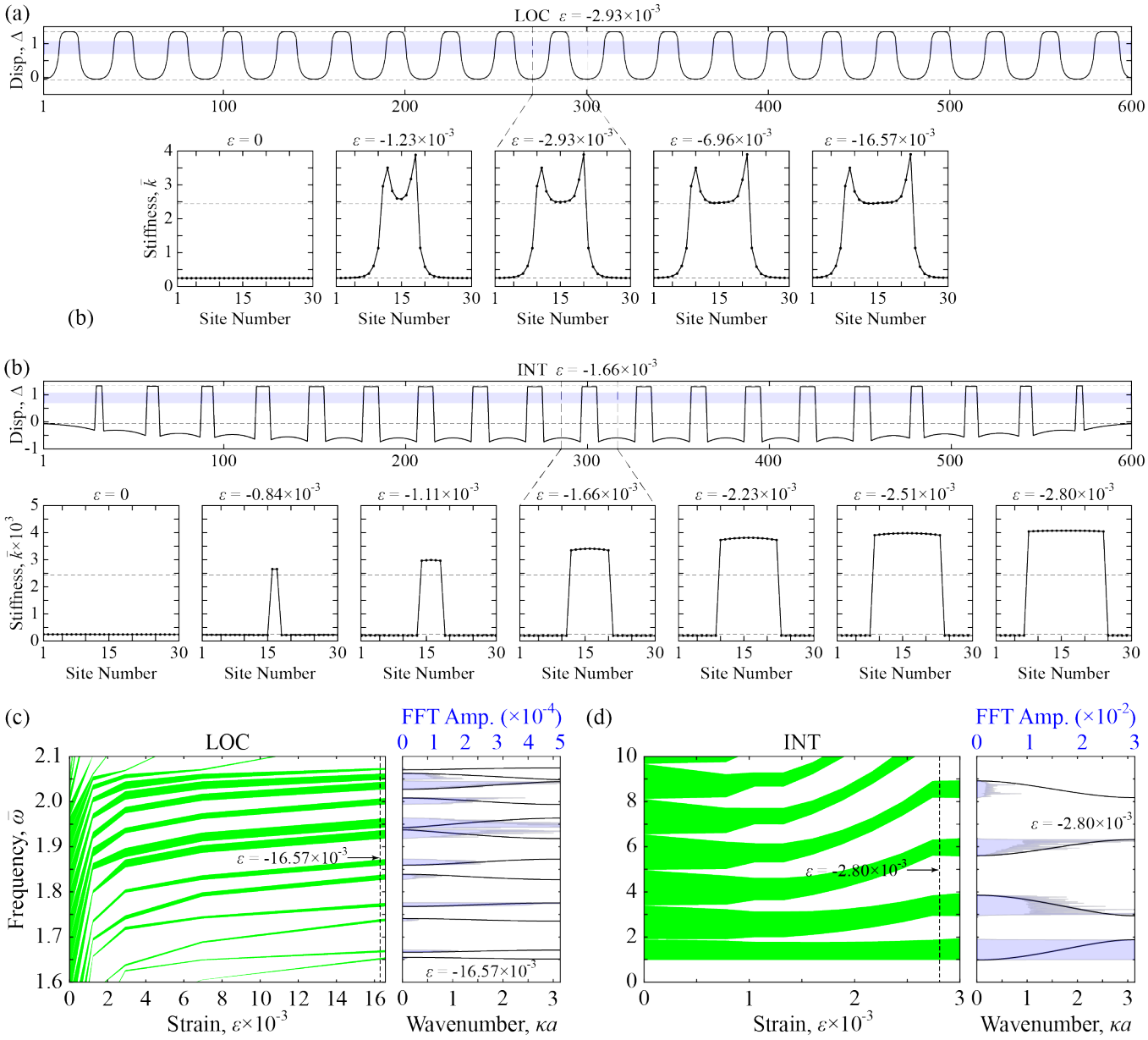

FIG. 5. (Color online). Metamaterial with Tunable Unit Cell Morphology. (a,b) Subject to boundary displacement, a substrate with periodic stiffness variation elicits a displacement profile, Δ_j, with similar periodicity, leading to periodic element re-configuration and stiffness modulation, $\bar{k}_j$. The (analytical) dispersion pass bands and the (numerical) FFT of a simulated disturbance are compared, revealing rough agreement for the (c) LOC system away from flat bands and excellent agreement for the (d) INT arrangement at lower frequencies.

IV. CONCLUSIONS

Typically, metamaterial tuning schemes demonstrate continuity, stability, or reversibility individually or in pair-wise but not triple combination. In this article, we propose a one-dimensional system comprised of a bistable metamaterial on an elastic substrate which permits continuous, stable, and reversible adjustments to the morphology through strain engineering and, thus, tunable dynamic performance. This is demonstrated in the form of a wave waveguide with variable pass band and a metamaterial unit cell with flexible morphology supporting a tunable dispersion. The strategy of strain engineering for morphological tuning can be extended to higher dimensions, however, the results are generally not stable[58,59] in the absence of persistent substrate strain. However, e.g., defects and the interaction of nonlinear wave modes with the transition zone represent two promising methods to overcome this obstacle. In addition, as s_j approaches $\bar{k}_1$, the substrate not only begins to participate in shaping the wave dynamics together

with the metamaterial but also begins to sustain an apparent deformation profile (i.e., warping) in the face of non-uniform metamaterial morphologies (see Supplementary Material). This effect suggests an alternative route to programming shape in soft matter[60].

SUPPLEMENTARY MATERIAL

See supplementary material for animations and further details of the tuning and potential recovery of the metamaterial in LOC and INT arrangements.

ACKNOWLEDGMENTS

This work is supported by start-up funds provided by the University of California.

DATA AVAILABILITY

The data that supports the findings of this study are available within the article and its supplementary material.

APPENDIX

Potential Function

Consider each term in Eq. (1) in turn. From the geometry illustrated in Fig. 1a, where $\delta = d_y/d_x$, the instantaneous length of an axial spring is $\ell(\Delta) = d_x\bar{\ell}(\Delta) = d_x\sqrt{(1-\Delta)^2+\delta^2}$ and, therefore, its natural length is $\ell_0 = d_x\bar{\ell}(0)$. Thus, the contribution of axial springs to the on-site potential is given by

$$\psi_A(\Delta) = k_A d_x^2\left[\bar{\ell}(\Delta) - \bar{\ell}_0\right]^2.$$

In general, for a dipole moment $\mathbf{p}$ in a magnetic field $\mathbf{B}$, the potential energy is given by $\psi_M = -\mathbf{p}\cdot\mathbf{B}$. The field $\mathbf{B}$ of an arbitrary, point-like magnetic dipole $\mathbf{p} = p\hat{\mathbf{p}}$ is[61,62]

$$\mathbf{B}(\mathbf{p},\mathbf{r}) = \frac{\mu_0 p}{4\pi|\mathbf{r}|^3}\left[\frac{3}{|\mathbf{r}|^2}(\hat{\mathbf{p}}\cdot\mathbf{r})\mathbf{r} - \hat{\mathbf{p}}\right],$$

where $\mathbf{r}$ is the position vector of a point in space relative to the position of the field-generating dipole and μ_0 is the permeability of free space. At present, the dipole moment under consideration is that affixed to the mass, $\mathbf{p}_m$, and $\mathbf{B}$ is that resulting from the superposition of fields generated by the $\mathbf{p}_s$ pair at the site of $\mathbf{p}_m$. To ensure a horizontal resultant, $\mathbf{p}_m$ remains parallel to the x-axis while the orientation, θ, of $\mathbf{p}_s$ is symmetric about the horizontal axis. For our system, the position vector can be written $\mathbf{r} = d_x\bar{\mathbf{r}}$ and the magnetic potential becomes

$$\psi_M = k_M d_x^2\sum_{i=1}^{2}\frac{\hat{\mathbf{p}}_m}{|\bar{\mathbf{r}}_i|^3}\cdot\left[\frac{3}{|\bar{\mathbf{r}}_i|^2}(\hat{\mathbf{p}}_{s(i)}\cdot\bar{\mathbf{r}}_i)\bar{\mathbf{r}}_i - \hat{\mathbf{p}}_{s(i)}\right],$$

where $k_M = \mu_0 p_s p_m/4\pi d_x^5$. Notice that the magnetic potential does not include contributions from dipole moments in neighboring bistable elements.

Finally, the torsional springs resist the angular displacement, $\varphi(\Delta)$, of the axial springs relative to some arbitrary offset, φ_0, and may be regarded as the bending resistance from the ends of the axial springs fixed to the substrate. For simplicity, $\varphi_0 = \tan^{-1}[(1-\Delta_{s(i)})/\delta]$, where the specific value of i is that for which $\Delta_{s(i)}$ is in the upper energy well of the total potential constructed from ψ_A and ψ_M alone; consequently,

$$\psi_T(\Delta) = k_T\left[\tan^{-1}\left(\tfrac{1-\Delta}{\delta}\right) - \tan^{-1}\left(\tfrac{1-\Delta_{s(i)}}{\delta}\right)\right]^2.$$

Following the normalization described in Sec. II B, we define $\bar{k}_A = k_A/k_I$, $\bar{k}_M = k_M/k_I$, and $\bar{k}_T = k_T/k_I d_x^2$.

Dispersion Relations

Following Eqs. (3) and (4), the matrix equations of motion for an arbitrary unit cell are given by:

$$\begin{bmatrix} 1 & -1 \\ -1 & 1+\bar{k}_{s(i)}-\bar{\omega}^2 \end{bmatrix}\begin{bmatrix}\bar{v}_{j-1}\\ \bar{v}_j\end{bmatrix} = \begin{bmatrix} f_{j-1}\\ f_j\end{bmatrix}, \quad \text{(LOC)}$$

$$\begin{bmatrix} \bar{k}_{s(i)} & -\bar{k}_{s(i)} \\ -\bar{k}_{s(i)} & 1+\bar{k}_{s(i)}-\bar{\omega}^2 \end{bmatrix}\begin{bmatrix}\bar{v}_{j-1}\\ \bar{v}_j\end{bmatrix} = \begin{bmatrix} f_{j-1}\\ f_j\end{bmatrix}, \quad \text{(INT)}$$

where f_j and f_{j-1} are the forces applied by the adjacent unit cells. Following Sec. II. A., the local stiffness is given by $\bar{k}(\Delta) = \partial^2\bar{\psi}/\partial\Delta^2$; therefore, $\bar{k}_{s(i)} = \bar{k}(\Delta_{s(i)})$ are the stiffnesses associated with the two stable configurations, $\Delta_{s(i)}$, $i = 1,2$. Recall, for the LOC arrangement, $\Delta = \bar{v}_j - \bar{V}_j$ and, for the INT arrangement, $\Delta = \bar{v}_{j-1} - \bar{v}_j$. Following Bloch's theorem, $\bar{v}_{j-1} = \bar{v}_j\gamma$, where $\gamma = e^{-i\kappa a}$ is the complex propagation constant with wavenumber κ. Thus, the displacement transformation $\left[\bar{v}_{j-1},\bar{v}_j\right]^T = \mathbf{T}\bar{v}_j$, where $\mathbf{T} = [\gamma \quad 1]^T$ is the Bloch transformation matrix. Simultaneously, pre-multiplying the matrix equations of motion by the conjugate transpose, $\mathbf{T}^H$, and applying the displacement transformation – recognizing that cell equilibrium requires $\mathbf{T}^H\mathbf{f} = \mathbf{0}$ – reduces the equation dimensions. The subsequent determinate establishes the metamaterial characteristic wave dispersion relations in Eqs. (5).

[1] M. Maldovan, "Sound and heat revolutions in phononics," Nature **503**, 209–217 (2013).
[2] M. I. Hussein, M. J. Leamy, and M. Ruzzene, "Dynamics of phononic materials and structures: historical origins, recent progress, and future outlook," Applied Mechanics Reviews **66**, 040802 (2014).
[3] D. M. Kochmann and K. Bertoldi, "Exploiting microstructural instabilities in solids and structures: from metamaterials to structural transitions," Appl. Mech. Rev. **69**, 050801 (2017).
[4] T. Han, T. Yuan, B. Li, and C.-W. Qiu, "Homogeneous thermal cloak with constant conductivity and tunable heat localization," Sci. Rep. **3**, 1593 (2013).
[5] T. Han, X. Bai, D. Gao, J. T. Thong, B. Li, and C.-W. Qiu, "Experimental demonstration of a bilayer thermal cloak," Phys. Rev. Lett. **112**, 054302 (2014).

[6] L. Xu, S. Yang, and J. Huang, "Passive metashells with adaptive thermal conductivities: chameleonlike behavior and its origin," Phys. Rev. Applied **11**, 054071 (2019).

[7] B. Deng, P. Wang, Q. He, V. Tournat, and K. Bertoldi, "Metamaterials with amplitude gaps for elastic solitons," Nat. Commun. **9**, 3410 (2018).

[8] N. X. Fang, D. Xi, J. Xu, M. Ambati, W. Srituravanich, C. Sun, and X. Zhang, "Ultrasonic metamaterials with negative modulus," Nature Materials **5**, 452–456 (2006).

[9] H. Yang and L. Ma, "Multi-stable mechanical metamaterials with shape-reconfiguration and zero Poisson's ratio," Materials & Design **152**, 181–190 (2018).

[10] G. Trainiti, Y. Xia, J. Marconi, G. Cazzulani, A. Erturk, and M. Ruzzene, "Time-periodic stiffness modulation in elastic metamaterials for selective wave filtering: theory and experiment," Phys. Rev. Lett. **122**, 124301 (2019).

[11] Y. Xie, W. Wang, H. Chen, A. Konneker, B.-I. Popa, and S. A. Cummer, "Wavefront modulation and subwavelength diffractive acoustics with an acoustic metasurface," Nat. Commun. **5**, 5553 (2014).

[12] A. Shelke, S. Banerjee, A. Habib, E. K. Rahani, R. Ahmed, and T. Kundu, "Wave guiding and wave modulation using phononic crystal defects," J. Intell. Mater. Syst. Struct. **25**, 1541–1552 (2013).

[13] N. Boechler, G. Theocharis, and C. Daraio, "Bifurcation-based acoustic switching and rectification," Nature Materials **10**, 665–668 (2011).

[14] B. Liang, X. S. Guo, J. Tu, D. Zhang, and J. C. Cheng, "An acoustic rectifier," Nature Materials **9**, 989–992 (2010).

[15] C. Ma, R. G. Parker, and B. B. Yellen, "Optimization of an acoustic rectifier for uni-directional wave propagation in periodic mass–spring lattices," J. Sound Vib. **332**, 4876–4894 (2013).

[16] R. A. Shelby, D. R. Smith, and S. Schultz, "Experimental verification of a negative index of refraction," Science **292**, 77–79 (2001).

[17] K. Sun, R. Fan, X. Zhang, Z. Zhang, Z. Shi, N. Wang, P. Xie, Z. Wang, G. Fan, H. Liu, C. Liu, T. Li, C. Yan, and Z. Guo, "An overview of metamaterials and their achievements in wireless power transfer," J. Mater. Chem. C **6**, 2925–2943 (2018).

[18] Z. Yang, J. Mei, M. Yang, N. H. Chan, and P. Sheng, "Membrane-type acoustic metamaterial with negative dynamic mass," Physical Review Letters **101**, 204301 (2008).

[19] S. A. Cummer and D. Schurig, "One path to acoustic cloaking," New Journal of Physics **9**, 45 (2007).

[20] N. Stenger, M. Wilhelm, and M. Wegener, "Experiments on elastic cloaking in thin plates," Physical Review Letters **108**, 014301 (2012).

[21] M. Ambati, N. Fang, C. Sun, and X. Zhang, "Surface resonant states and superlensing in acoustic metamaterials," Physical Review B **75**, 195447 (2007).

[22] O. R. Bilal, A. Foehr, and C. Daraio, "Bistable metamaterial for switching and cascading elastic vibrations," Proc. Natl. Acad. Sci. **114**, 4603–4606 (2017).

[23] J.-F. Robillard, K. Muralidharan, J. Bucay, P. A. Deymier, W. Beck, and D. Barker, "Phononic metamaterials for thermal management: an atomistic computational study," Chin. J. Phys. **49**, 448–461 (2011).

[24] R. Schittny, M. Kadic, S. Guenneau, and M. Wegener, "Experiments on transformation thermodynamics: molding the flow of heat," Phys. Rev. Lett. **110**, 195901 (2013).

[25] Y. Pennec, B. Djafari-Rouhani, J. O. Vasseur, A. Khelif, and P. A. Deymier, "Tunable filtering and demultiplexing in phononic crystals with hollow cylinders," Physical Review E **69**, 046608 (2004).

[26] R. Fleury, D. Sounas, and A. Alu, "An invisible acoustic sensor based on parity-time symmetry," Nat. Commun. **6** (2015), 10.1038/ncomms6905.

[27] X. Wang, J. Xu, J. Ding, C. Zhao, and Z. Huang, "A compact and low-frequency acoustic energy harvester using layered acoustic metamaterials," Smart Mater. Struct. **28**, 025035 (2019).

[28] C.-S. Park, Y. C. Shin, S.-H. Jo, H. Yoon, W. Choi, B. D. Youn, and M. Kim, "Two-dimensional octagonal phononic crystals for highly dense piezoelectric energy harvesting," Nano Energy **57**, 327–337 (2019).

[29] J. Henneberg, A. Gerlach, H. Cebulla, and S. Marburg, "The potential of stop band material in multi-frequency ultrasonic transducers," J. Sound Vib. **452**, 132–146 (2019).

[30] A. Colombi, D. Colquitt, P. Roux, S. Guenneau, and R. V. Craster, "A seismic metamaterial: the resonant metawedge," Sci. Rep. **6**, 27717 (2016).

[31] S. Brûlé, E. H. Javelaud, S. Enoch, and S. Guenneau, "Experiments on seismic metamaterials: molding surface waves," Phys. Rev. Lett. **112**, 133901 (2014).

[32] O. Thorp, M. Ruzzene, and A. Baz, "Attenuation and localization of wave propagation in rods with periodic shunted piezoelectric patches," Smart Mater. Struct. **10**, 979–989 (2001).

[33] L. Airoldi and M. Ruzzene, "Design of tunable acoustic metamaterials through periodic arrays of resonant shunted piezos," New J. Phys. **13**, 113010 (2011).

[34] B.-J. Kwon, J.-Y. Jung, D. Lee, K.-C. Park, and I.-K. Oh, "Tunable acoustic waveguide based on vibro-acoustic metamaterials with shunted piezoelectric unit cells," Smart Mater. Struct. **24**, 105018 (2015).

[35] P. Celli and S. Gonella, "Tunable directivity in metamaterials with reconfigurable cell symmetry," Appl. Phys. Lett. **106**, 091905 (2015).

[36] F. Li, C. Zhang, and C. Liu, "Active tuning of vibration and wave propagation in elastic beams with periodically placed piezoelectric actuator/sensor pairs," J. Sound Vib. **393**, 14–29 (2017).

[37] G. Wang, J. Cheng, J. Chen, and Y. He, "Multi-resonant piezoelectric shunting induced by digital controllers for subwavelength elastic wave attenuation in smart metamaterial," Smart Mater. Struct. **26**, 025031 (2017).

[38] C. Daraio, V. F. Nesterenko, E. B. Herbold, and S. Jin, "Tunability of solitary wave properties in one-dimensional strongly nonlinear phononic crystals," Phys. Rev. E **73**, 026610 (2006).

[39] K. Bertoldi and M. C. Boyce, "Mechanically triggered transformations of phononic band gaps in periodic elastomeric structures," Phys. Rev. B **77**, 052105 (2008).

[40] X. Zhu, G. Wu, R. Dong, C.-M. Chen, and S. Yang, "Capillarity induced instability in responsive hydrogel membranes with periodic hole array," Soft Matter **8**, 8088–8093 (2012).

[41] C. R. Tipton, E. Han, and T. Mullin, "Magneto-elastic buckling of a soft cellular solid," Soft Matter **8**, 6880–6883 (2012).

[42] P. Wang, F. Casadei, S. Shan, J. C. Weaver, and K. Bertoldi, "Harnessing buckling to design tunable locally resonant acoustic metamaterials," Phys. Rev. Lett. **113**, 014301 (2014).

[43] F. Casadei and K. Bertoldi, "Harnessing fluid-structure interactions to design self-regulating acoustic metamaterials," J. Appl. Phys. **115**, 034907 (2014).

[44] S. Shan, S. H. Kang, P. Wang, C. Qu, S. Shian, E. R. Chen, and B. Katia, "Harnessing multiple folding mechanisms in soft periodic structures for tunable control of elastic waves," Adv. Funct. Mater. **24**, 4935–4942 (2014).

[45] A. Rafsanjani and K. Bertoldi, "Buckling-induced kirigami," Phys. Rev. Lett. **118**, 084301 (2017).

[46] D. Yang, L. Jin, R. V. Martinez, K. Bertoldi, G. M. Whitesides, and Z. Suo, "Phase-transforming and switchable metamaterials," Extreme Mech. Lett. **6**, 1–9 (2016).

[47] A. Rafsanjani and D. Pasini, "Bistable auxetic mechanical metamaterials inspired by ancient geometric motifs," Extreme Mech. Lett. **9**, 291–296 (2016).

[48] J. R. Raney, N. Nadkarni, C. Daraio, D. M. Kochmann, J. A. Lewis, and K. Bertoldi, "Stable propagation of mechanical signals in soft media using stored elastic energy," Proc. Natl. Acad. Sci. **113**, 9722–9727 (2016).

[49] M. J. Frazier and D. M. Kochmann, "Band gap transmission in periodic bistable mechanical systems," J. Sound Vib. **388**, 315–326 (2017).

[50] J. Meaud and K. Che, "Tuning elastic wave propagation in multistable architected materials," Int. J. Solids Struct. **122–123**, 69–80 (2017).

[51] J. Meaud, "Multistable two-dimensional spring-mass lattices with tunable band gaps and wave directionality," J. Sound Vib. **434**, 44–62 (2018).

[52] Z. Wu, Y. Zheng, and K. W. Wang, "Metastable modular metastructures for on-demand reconfiguration of band structures and nonreciprocal wave propagation," Phys. Rev. E **97**, 022209 (2018).

[53] X. Xia, A. Afshar, H. Yang, C. M. Portela, D. M. Kochmann, C. V. Di Leo, and J. R. Greer, "Electrochemically reconfigurable architected materials," Nature **573**, 205–213 (2019).

[54] G. Catalan, A. Lubk, A. H. G. Vlooswijk, E. Snoeck, C. Magen Dominguez, A. Janssens, G. Rispens, G. Rijnders, D. H. A. Blank, and B. Noheda, "Flexoelectric rotation of polarization in ferroelectric thin films," Nat. Mater. **10**, 963–967 (2011).

[55] Z. Dai, L. Liu, and Z. Zhang, "Strain engineering of 2D materials: issues and opportunities at the interface," Adv. Mater. **0**, 1805417 (2019).

[56]N. Nadkarni, C. Daraio, and D. M. Kochmann, "Dynamics of periodic mechanical structures containing bistable elastic elements: From elastic to solitary wave propagation," Physical Review E **90**, 023204 (2014).

[57]For the LOC arrangement, the interaction springs prevent the transition region from advancing beyond the midpoint. The INT arrangement is not so limited.

[58]S. M. Allen and J. W. Cahn, "A microscopic theory for antiphase boundary motion and its application to antiphase domain coarsening," Acta Metall. **27**, 1085–1095 (1979).

[59]M. J. Frazier and D. M. Kochmann, "Atomimetic mechanical structures with nonlinear topological domain evolution kinetics," Adv. Mater. , 1605800 (2017).

[60]S. Janbaz, R. Hedayati, and A. A. Zadpoor, "Programming the shape-shifting of flat soft matter: from self-rolling/self-twisting materials to self-folding origami," Mater. Horiz. **3**, 536–547 (2016).

[61]K. W. Yung, P. B. Landecker, and D. D. Villani, "An analytic solution for the force between two magnetic dipoles," Magnetic and Electrical Separation **9**, 39–52 (1998).

[62]D. J. Griffiths, *Introduction to Electrodynamics* (Boston: Pearson, 2013).